Lithuanian Journal of Physics
Vol. **65**, No. 3, pp. 137–146 (2025)
ISSN 1648-8504 eISSN 2424-3647
DOI: https://doi.org/10.3952/physics.2025.65.3.2

NONHOMOGENEOUSLY POLARIZED AIRY BEAMS AND THEIR ACCELERATING LATTICES OF OPTICAL QUASIPARTICLES

J. Berškys, K. Laurinavičius, and S. Orlov

Coherent Optics Laboratory, State Research Institute Center for Physical Sciences and Technology, Saulėtekio 3, 10257 Vilnius, Lithuania
Email: justas.berskys@ftmc.lt; sergejus.orlovas@ftmc.lt

Received 24 June 2025; revised 21 August 2025; accepted 15 September 2025

Radially polarized Airy vector beams are numerically investigated in terms of their spatial spectra, electromagnetic field distribution, and topological structure. Airy-type beams, which belong to the class of non-diffracting optical beams, are notable for their ability to propagate in a bent accelerating trajectory while reconstructing their intensity profiles even after encountering obstructions. This work analytically investigates vector beams with non-uniform, radial and azimuthal polarization distributions, which exhibit phase singularities and intensity zeros (dark spots). Additional topological features are observed, and the skyrmionic density of the electric field and the linear momentum are analyzed numerically, revealing the existence of an accelerating lattice of optical quasiparticles in the beams.

Keywords: Airy beams, polarization, topological quasiparticles

1. Introduction

Electromagnetic waves are characterized by four main parameters: wavelength, phase, polarization and amplitude. Advances in lasers, optical elements and meta-elements [1, 2] have driven developments in metrology, manufacturing and quantum technologies. Manipulating these parameters enables the creation of diverse optical fields, from optical tweezers [3] and Möbius strips to non-diffracting beams [5, 6] and topological particles of light [7, 8].

Non-diffracting beams, such as Bessel and Airy beams, exhibit properties such as robustness to environmental perturbations [9], and can carry the angular momentum, which can be transferred to nanoparticles. Polarization manipulation significantly affects the propagation dynamics of optical fields [10], leading to such phenomena as singular polarization beams [11] and spin–orbit interactions [12].

Topological quasiparticles, or skyrmions, first proposed by Skyrme [13], have gained attention in various fields, including optics [14]. They can be observed in the Stokes field domain [15], electric field [16], and in the spin of light [17].

Optical quasiparticles have been explored in optical lattices [18], light pulses [19] and photonic hopfions [20]. Optical skyrmionic beams are invariant propagation modes, so these topological structures are robust [21] and can be used for applications that require robust information transfer [22].

Optical lattices with topological quasiparticles, rooted in phase singularities, have been studied using Bessel beams [23]. Periodic skyrmionic structures with propagation-invariant properties and Airy beams with polarization singularities [24] have been observed. The topological lattice structure has been observed in meron lattices [25, 26], and was also demonstrated in nonhomogeneously polarized Airy-like beams, where superposition of left- and right-hand circularly polarized Airy beams with a phase difference was used to generate such lattices [27]. Periodic topological structures in free-space beams can lead to applications in creating spin textures in Bose–Einstein

condensates [28], potential data storage and information transfer applications [29, 30], or nontrivial light–matter interactions [31].

In this research, we build upon our previous workf [24] and continue the investigation of radially and azimuthally polarized Airy-like beams. The goal is to analyze their electric field distributions, spatial spectra, and second-order forms of the electromagnetic field (such as linear momentum). Furthermore, we theoretically investigate their topological structure and identify the topological configurations associated with these beams, ultimately revealing the existence of an accelerating lattice of optical quasiparticles within them.

The problem that we address here is the absence of a detailed theoretical and numerical characterization of these topological structures in nonhomogeneously polarized Airy beams, which this work aims to provide.

2. Theoretical background

When electromagnetic fields are investigated, their polarization properties are attributed by assuming a linear, circular, or elliptical polarization state homogeneously overlaying the transverse distribution of the field. Suppose that nonhomogeneous polarization states are considered when the electromagnetic field in the transverse plane has a different type of polarization state. In that case, solving Maxwell's equations of a propagating light field might become a difficult task.

One of the approaches to finding orthogonal solutions to propagating fields is described by Stratton [32]. If an isotropic medium without any charges is considered, the electric **E** and magnetic **B** fields follow the same differential equation. When the time dependence $e^{-i\omega t}$ is factored out and **C** denotes the electric or magnetic fields, then the wave equation is given by

$$\nabla \cdot \mathbf{C} - \nabla \times \nabla \times \mathrm{C} + k^2\mathbf{C} = 0. \tag{1}$$

Let the scalar function ψ be a solution to the scalar wave equation:

$$\nabla^2\psi + k^2\psi = 0. \tag{2}$$

From the scalar function ψ one can construct three orthogonal vector fields: **L**, **M** and **N** [33]:

$$\mathbf{L} = \nabla\psi,\ \mathbf{M} = \nabla \times \mathbf{a}\psi,\ \mathbf{N} = \frac{1}{k}\nabla \times \mathbf{M}. \tag{3}$$

Here **a** is a specific vector that determines the symmetry of the vector fields **L**, **M** and **N**. If these vector fields are used instead of the field **C**, it can be proved that they satisfy the vector wave equation (1). In this case, any scalar field solution of a scalar wave function can be used to construct three orthogonal vector fields. Particular interest is given to the vector fields **M** and **N** as they are solenoidal:

$$\nabla \cdot \mathbf{M} = 0,\ \nabla \cdot \mathbf{N} = 0. \tag{4}$$

Here we use the Airy beam, a solution of the scalar wave equation in paraxial approximation conditions, as a scalar function to construct vector fields, given by

$$u_t(s_t, \xi_t) = \mathrm{Ai}\,[s_t - (\xi_t/2)^2 + \mathrm{i}a_t\xi_t] \times$$

$$\times \exp\,[a_t(s_t - \xi_t^2/2) + \mathrm{i}\xi_t/2(a_t^2 + s_t - \xi_t^2/6)]. \tag{5}$$

The solution for (2+1)D is obtained straightforwardly from the solution of (1+1)D:

$$\psi(x, y, z), = \prod_{t=x,y} u_t(s_t, \xi_t). \tag{6}$$

Here $s = x/x_0$ is a transverse component of the beam, x_0 is an arbitrary transverse scale, $\xi = z/kx_0^2$ is a normalized propagation distance, and $k = 2\pi n/\lambda_0$ is the wave number of the beam with the refractive index of the environment n and λ_0, a wavelength of the optical field. This expression shows an apertured Airy beam with the decay factor a. Authors make a note here that in the numerical simulations, all spatial quantities are expressed in dimensionless normalized units. The physical dimensions are obtained by scaling with the chosen transverse normalization factors x_0 and y_0, which can be set for any given value. In this normalization, the physical wavelength λ_0 is proportional to normalization factors, allowing it to be chosen in the optical range. This normalization simplifies the analysis, keeps the results general, and allows easy rescaling to different wavelength regimes.

In this work, we investigate the properties of the vector fields **M** and **N**, which are constructed using an arbitrarily chosen radial symmetry vector field **a** = (*x*, *y*, *z*). These two orthogonal vector field

solutions are derived by substituting the apertured Airy beam, given in Eq. (6), a solution to the scalar wave equation (2) under the paraxial wave approximation, into Eq. (3). The choice of selecting an arbitrary vector to be radially polarized is based on the fact that, in such a way, a promising and rich field structure can be found. While linearly polarized Airy beams have been extensively studied for their self-accelerating and non-diffracting properties, they lack the complex polarization singularities and a spatially varying vectorial structure that arise in nonhomogeneously polarized beams.

In Fig. 1, the 3D isointensity plots of the vector field modes **M** and **N** are depicted. Here we choose the wavenumber $k = 2\pi$, the decay parameters $a_x = a_y = 0.2$, and the transverse normalization component of the beams $x_0 = y_0 = 1$. The three different colours in the plot correspond to the different isointensity surfaces for the normalized intensity of the beams. The propagation of the parabolic shape is visible for both the **M** and **N** beams, which is a distinguishing feature of a scalar Airy beam. The red lines show the direction of the electric field. For the beam of type **M**, this corresponds to the transverse electric mode (TE), and the field lines are enclosed. However, for the **N** type beam, the electric field direction is transverse magnetic (TM), and this corresponds to the out-/ingoing electric field direction.

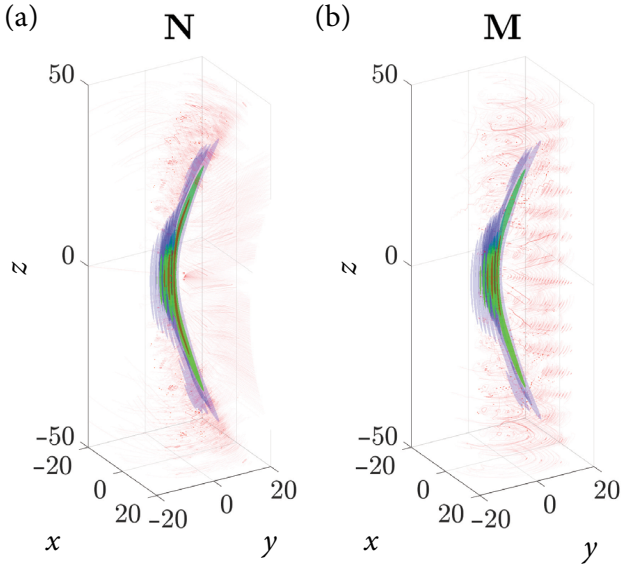

Fig. 1. (a) Three-dimensional isointensity surfaces of the transverse electric (**N**) and (b) of the transverse magnetic (**M**) vector Airy beams. Parameters are $\mathbf{a}_K$, with decay parameter $a_x = a_y = 0.2$. The intensities are normalized to maximal values, the scale parameters are $x_0 = y_0 = 1$, and the wavenumber is $k = 2\pi$. The red streamlines represent the electric field in the vicinity of the beam.

The absolute value of the electric field and its constituent vector components in the $\mathbf{e}_x$, $\mathbf{e}_y$ and $\mathbf{e}_z$ directions are shown in Fig. 2. The first two plots 2 (a) and (b) correspond to the normalized absolute value of the **M** and **N** type beams at the propagation distance $z = 0$, where the white arrows represent an electric field direction. From this cross-section few observations can be made. First, both vector modes have a similar amplitude distribution, corresponding to the scalar Airy beam. Moreover, the main lobe is disrupted by the point-like polarization singularity. The field lines for the **M** type beam are oriented azimuthally, and for the **N** type beam they are oriented radially.

Next, the different vector field components for the **M** type and **N** type beams are presented in Fig. 2(c–e) and (f–h), respectively. It is observed that for both beams, the $\mathbf{e}_x$ component can be matched to the $\mathbf{e}_y$ component by rotation over the $y = x$ axis. Furthermore, the absolute value of the amplitude of the $\mathbf{M}_x$ component is identical to the component of $\mathbf{M}_y$ beam, and the $\mathbf{M}_y$ to the $\mathbf{N}_x$. The $\mathbf{M}_z$ and $\mathbf{N}_z$ components do not share similarities and are unique for each beam.

The angular spectra of these beams are presented in Fig. 3 to illustrate their far-field structure, which is given by the spatial Fourier transform of the field distribution. We can draw similar conclusions to those from the investigation of the cross-sections of the electric field distribution. The orthogonal components of $\mathbf{e}_x$ and $\mathbf{e}_y$ for different beams are similar with an additional phase difference, and vice versa. The main differing factor comes from an $\mathbf{e}_z$ component for both beams.

3. Topological quasiparticles

In this section, we focus on the topological structure of **M** and **N** type beams. Skyrmions are stable topologically confined field configurations first described by Skyrme in the context of particle physics [13, 34]. This investigation is usually carried out by mapping the field on a unit sphere S^2 to the points of a 2D plane; such 2D field configurations are usually called 'baby skyrmions'. The normalized vector

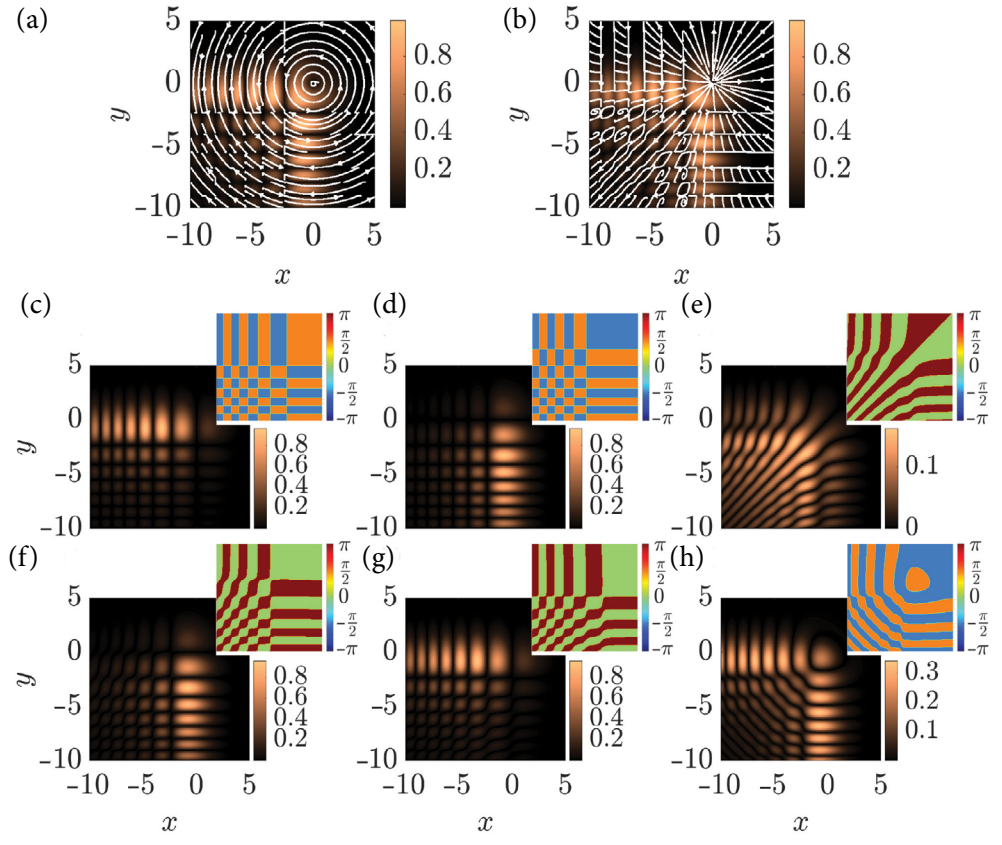

Fig. 2. (a, c–e) The absolute value of the electric field amplitude distributions of **M** and (b, f–h) of the **N** beam. (a, b) The total intensity at $z = 0$, white arrows represent the flow of the vector field. The absolute value of the amplitude distribution of the components (c, f) $\mathbf{e}_x$, (d, g) $\mathbf{e}_y$ and (e, h) of the component $\mathbf{e}_z$ of the beams. The decay factors $a_x = a_y = 0.2$, the normalization distances $x_0 = y_0 = 1$ and the wavenumber $k = 2\pi$. Insets: phase distributions of the given components.

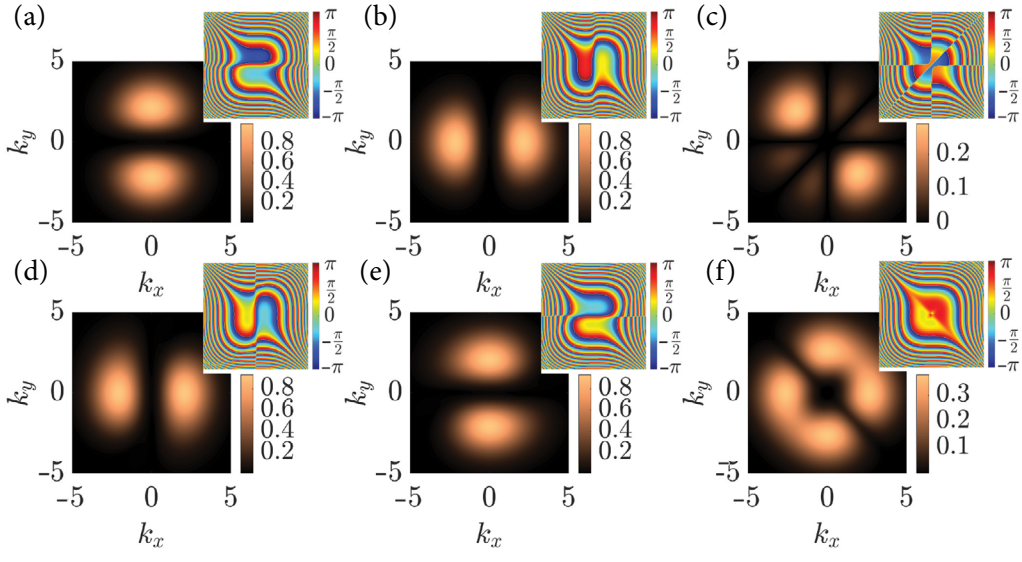

Fig. 3. (a–c) The angular spectrum of the vector field **M** and (d–f) of the vector field **N**. (a, d) The absolute value of the amplitude for the component $\mathbf{e}_x$ (b, e), $\mathbf{e}_y$ and (c, f) for the components $\mathbf{e}_z$. Wavenumber $k = 2\pi$, decay parameters $a_x = a_y = 0.2$. Insets: the distribution of the phase for the given components.

field $\mathbf{n}(\mathbf{r})$ can be selected to be any form (linear or quadratic) of the electromagnetic field, for example, the Stokes domain or the polarization domain of the fields. The topological density of a normalized field is given by

$$\rho_s(\mathbf{r}) = \mathbf{n}(\mathbf{r}) \cdot \left(\frac{\partial \mathbf{n}(\mathbf{r})}{\partial x} \times \frac{\partial \mathbf{n}(\mathbf{r})}{\partial y} \right). \tag{7}$$

We start by choosing the vector $\mathbf{a}$ to be $\mathbf{a} = \mathbf{a}_R$, where $\mathbf{a}_R = (x, y, z)$ is a radial vector of the spherical coordinate system.

Next, the distribution of the normalized electric field for the Airy vector beam at one particular distance is depicted in Fig. 4. The figure shows three portrayed plots: (a) the skyrmionic density of the normalized Re{**N**} type vector field, (b) the distribution of angles and z component directions, and (c) the absolute value of the normalized electric field in the direction of propagation. The streamlines indicate field direction in the transverse plane. The parameters used for the calculation are the decay factor $a_x = a_y = 0.16$, the normalization distances $x_0 = y_0 = 1$, the distance from the focus $z = 4$, the wavenumber $k = 2\pi$, and the normalized field is chosen to be $\mathbf{n} = \mathrm{Re}\{\mathbf{N}\}/|\mathbf{N}|$. In the density plot, see Fig. 4(a), one can observe small-scale density fluctuations, which indicate that topologically interesting configurations are present. Figure 4(b, c) helps one to understand the underlying arrangement of the vector field constructing such topological quasiparticles. We note that this topological structure moves with an acceleration inside the electromagnetic field [24].

In this field configuration, three types of different topological structures can be observed, see Fig. 5. The first is presented in Fig. 5 5(a–c), it resembles a topological state that has a single density maximum (Fig. 5(a)), but the z component has two oppositely directed peaks with the positively directed one being stronger (Fig. 5(b)). The transversal angular structure is shown in Fig. 5(c). It shows that the vector field is swirling around the positively directed z component. This attribute, in addition to the two oppositely directed z components, shows that the topological quasiparticle might be indicated as a Bloch-type bimeron configuration. The second intricate topological configuration observed is presented in Fig. 5(d–f). Here, the field distribution is similar to the one presented in Fig. 5(a–c), where the field is constructed out of the two-way oriented z component, but in this case, the swirling of the field is around the negatively directed longitudinal component (Fig. 5(f)). The topological density, see Fig. 5(e), has a negative value. Note that not the absolute value of the density *per se* is important, but the density that is rather positive than negative. The configuration of the field dictates that the attributed topological configuration is identified as a Bloch-type bimeron, but with a charge opposite to the one presented before. The third observed configuration, see Fig. 5(g–h), is also described with a positive single-density peak, see Fig. 5(g).

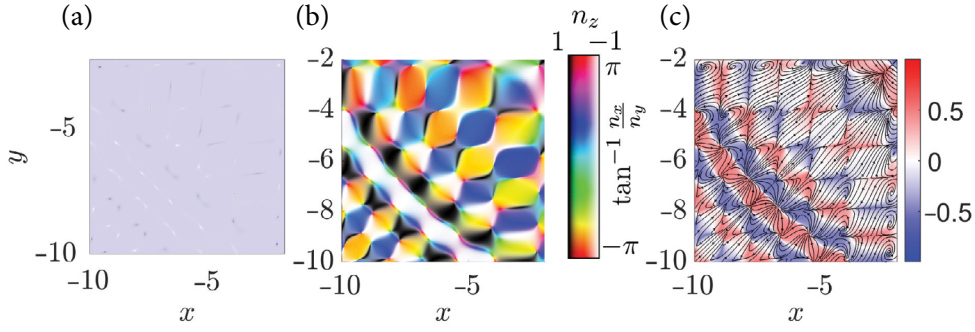

Fig. 4. Topological structure distribution of the real part of the vector field **N** when $n_x = \mathrm{Re}\{N_x\}/|\mathbf{N}|$, $n_y = \mathrm{Re}\{N_y\}/|\mathbf{N}|$ and $n_z = \mathrm{Re}\{N_z\}/|\mathbf{N}|$. The skyrmionic density (a), the distribution of the transverse components' angle (hue colour scheme) and the magnitude of the longitudinal component (black and white colour scheme) (b). The magnitude of the longitudinal component, where the black streamlines with arrows show the orientation of the transverse field (c). The parameters of the simulation are: the decay factors $a_x = a_y = 0.16$, the normalization distances $x_0 = y_0 = 1$, the distance from the focus $z = 4$ and the wavenumber $k = 2\pi$.

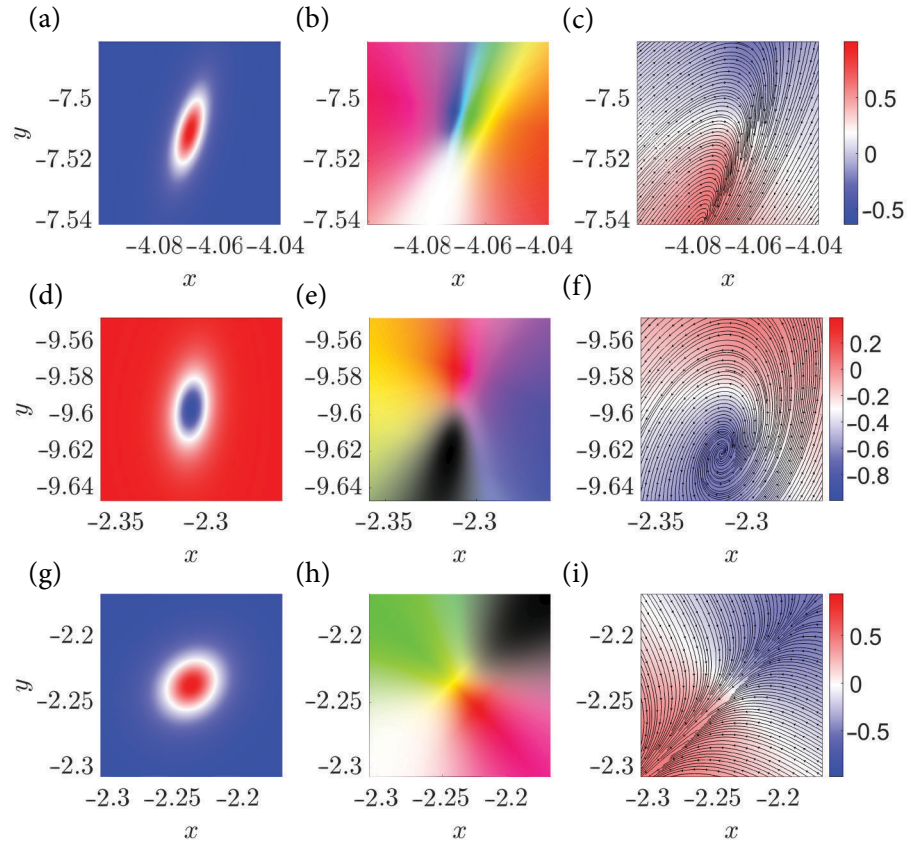

Fig. 5. Topological particles of the real part of the vector field **N** when $n_x = \mathrm{Re}\{N_x\}/|\mathbf{N}|$, $n_y = \mathrm{Re}\{N_y\}/|\mathbf{N}|$ and $n_z = \mathrm{Re}\{N_z\}/|\mathbf{N}|$. The skyrmionic density (a, d, g), the distribution of the transverse components' angle (hue colour scheme) and the magnitude of the longitudinal component (black and white colour scheme, see Fig. 4(b)) (b, e, h). The magnitude of the longitudinal component, where the black streamlines with arrows show the orientation of the transverse field (c, f, i). The parameters of the simulation are: the decay factors $a_x = a_y = 0.16$, the normalization distances $x_0 = y_0 = 1$, the distance from the focus $z = 4$ and the wavenumber $k = 2\pi$.

The distribution of the angle between the transversal components and the intensity of the z component is given in Fig. 5(h, i). The field has two identical intensity peaks pointing in opposite directions, the field around the positive z component seems to be a hedgehog-like distribution, and around the negative z component it is saddle-like. This provides information that the topological particle is a Néel-type bimeron.

In this part, the topological structure of the normalized linear momentum $\mathbf{n} = \mathrm{Re}\{\mathbf{P}\}/|\mathbf{P}|$ of the transverse magnetic field is investigated. The distributions of topological density and two graphs of vector distributions **n** are given in Fig. 6. In the density plot, Fig. 6(a), local small-scale positive and negative peaks are observed, indicating the field's topological particle existence. Vector plots, Fig. 6(b, c), show a grid-like structure with cells having the z component positively or negatively directed. However, there are a couple of regions in which the positive or negative z component does not cover all cells but is only locally present.

Further, three different topological particle configurations are observed and presented in Fig. 7. The first configuration is given in Fig. 7(a–c). The first image depicts the positive topological density of the particle. Figure 7(b, c) indicates that the orientation of the z component is oriented in the negative direction and the field is flowing into the centre of the particle. This behaviour is prominent and manifests in Néel-type skyrmionic

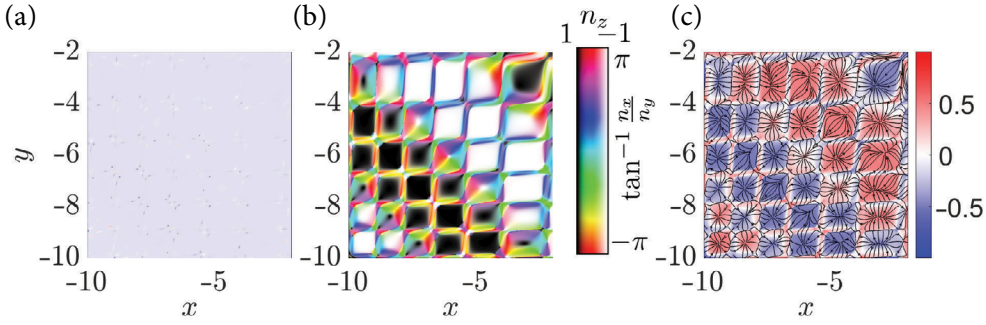

Fig. 6. Topological structure distribution of the real part of the linear momentum vector field **P** when $n_x = \mathrm{Re}\{P_x\}/|\mathbf{P}|$, $n_y = \mathrm{Re}\{P_y\}/|\mathbf{P}|$ and $n_z = \mathrm{Re}\{P_z\}/|\mathbf{P}|$. The skyrmionic density (a), the distribution of the transverse components' angle (hue colour scheme) and the magnitude of the longitudinal component (black and white colour scheme) (b). The magnitude of the longitudinal component, where the black streamlines with arrows show the orientation of the transverse field (c). The parameters of the simulation are: the decay factors $a_x = a_y = 0.16$, the normalization distances $x_0 = y_0 = 1$, the distance from the focus $z = 4$ and the wavenumber $k = 2\pi$.

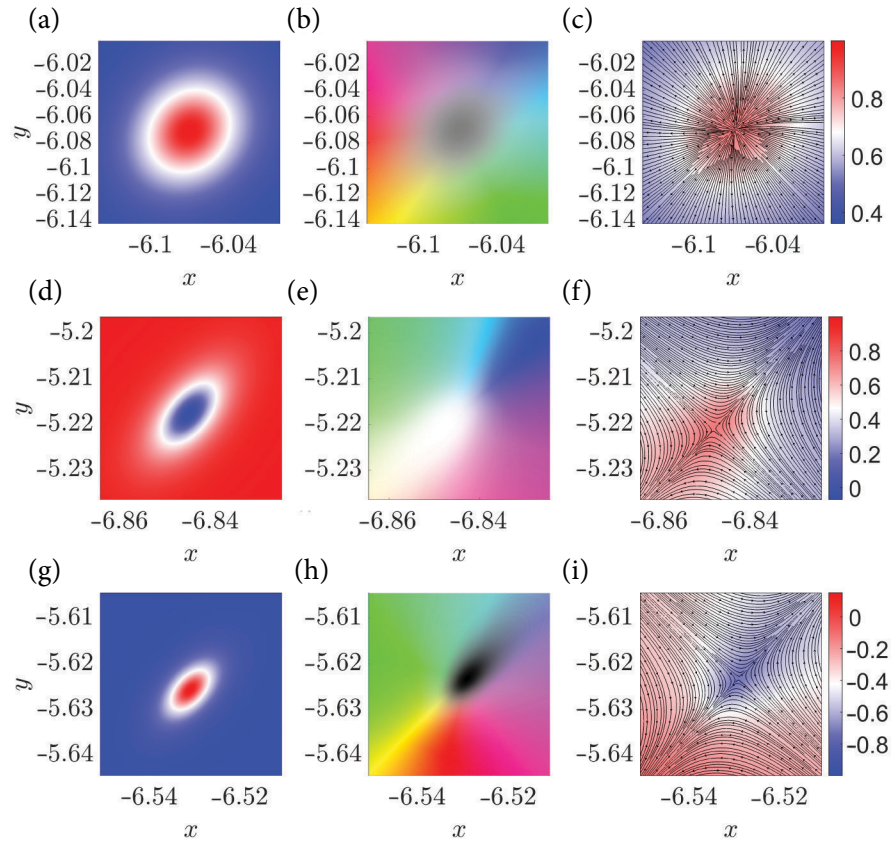

Fig. 7. Topological particles of the real part of the linear momentum vector field **P** when $n_x = \mathrm{Re}\{P_x\}/|\mathbf{P}|$, $n_y = \mathrm{Re}\{P_y\}/|\mathbf{P}|$ and $n_z = \mathrm{Re}\{P_z\}/|\mathbf{P}|$. The skyrmionic density (a, d, g), the distribution of the transverse components' angle (hue colour scheme) and the magnitude of the longitudinal component (black and white colour scheme, see Fig. 6(b)) (b, e, h). The magnitude of the longitudinal component, where the black streamlines with arrows show the orientation of the transverse field (c, f, i). The parameters of the simulation are: the decay factors $a_x = a_y = 0.16$, the normalization distances $x_0 = y_0 = 1$, the distance from the focus $z = 4$ and the wavenumber $k = 2\pi$.

particles, where the field around the peak is described as a hedgehog structure.

The second topological configuration is given in Fig. 7(d–f). In this part of the field, the observed skyrmionic density is negative, see Fig. 7(d). The field is oriented in a positive z direction, and the flow of the field around the peak has a saddle point, see Fig. 7(e, f). This arrangement of vectors indicates the topological quasiparticle described as an anti-skyrmion.

The third observed quasiparticle is shown in Fig. 7(g–i). Similar to the previous one, this particle has an opposite topological density, see Fig. 7(g), and the field has a saddle point in the vicinity of the positively directed z component. This feature of the configuration of the vector field gives insight into the localized particle as also an anti-skyrmion, with the field oriented in the opposite direction from the one presented in Fig. 7(d–f).

In general, these topological structures are evolving together with the electromagnetic field, so the topologically protected quasiparticles are located in the parabolic trajectory where the skyrmionic density is present. Moreover, these structures form similar to lattice-looking structures in their transversal profile.

4. Conclusions

In conclusion, an in-depth topological investigation of nonhomogeneously polarized Airy-like vector beams was conducted.

First, we review the analytical derivation procedure for orthogonal vector modes in radial symmetry, by the usage of scalar Airy beams – a solution of the paraxial wave equation. Moreover, a single distinct scalar Airy feature – an elongated intensity lobe – is present due to the interaction of the curved propagation trajectory with a point-like polarization singularity, located in the focal point. Theoretically, the Fourier spectra were analyzed. Our analysis revealed that the beam spectra of nonhomogeneously polarized Airy beams contain field components oriented along $\mathbf{e}_x$, $\mathbf{e}_y$, and the longitudinal direction $\mathbf{e}_z$.

Lastly, we continued by investigating the topological structure of the beam. When investigating the electric field domain of the **N** type beam, a Bloch-type bimeron configuration was found, as well as a Néel-type bimeron. In the domain of the real part of the linear momentum vector field, we observed Néel-type skyrmionic topological quasi-particles and anti-skyrmions appearing as an accelerating lattice.

In summary, this work provides the community with a comprehensive investigation into the topological properties of nonhomogeneously polarized vector Airy beams.

References

[1] A.H. Dorrah and F. Capasso, Tunable structured light with flat optics, Science **376**, eabi6860 (2022).

[2] Y. Shimotsuma, P.G. Kazansky, J. Qiu, and K. Hirao, Self-organized nanogratings in glass irradiated by ultra-short light pulses, Phys. Rev. Lett. **91**, 247405 (2003).

[3] Y. Yang, Y.-X. Ren, M. Chen, Y. Arita, and C. Rosales-Guzmán, Optical trapping with structured light: a review, Adv. Photonics **3**, 034001 (2021).

[4] T. Bauer, P. Banzer, E. Karimi, S. Orlov, A. Rubano, L. Marrucci, E. Santamato, R.W. Boyd, and G. Leuchs, Observation of optical polarization Möbius strips, Science **347**, 964 (2015).

[5] J. Durnin, J. Miceli Jr, and J.H. Eberly, Diffraction-free beams, Phys. Rev. Lett. **58**, 1499 (1987).

[6] D. McGloin and K. Dholakia, Bessel beams: Diffraction in a new light, Contemp. Phys. **46**, 15 (2005).

[7] D. Sugic, R. Droop, E. Otte, D. Ehrmanntraut, F. Nori, J. Ruostekoski, C. Denz, and M.R. Dennis, Particle-like topologies in light, Nat. Commun. **12**, 1 (2021).

[8] Y. Shen, Q. Zhang, P. Shi, L. Du, X. Yuan, and A.V. Zayats, Optical skyrmions and other topological quasiparticles of light, Nat. Photonics **18**, 15 (2024).

[9] J. Broky, G.A. Siviloglou, A. Dogariu, and D.N. Christodoulides, Self-healing properties of optical Airy beams, Opt. Express **16**, 12880 (2008).

[10] R. Dorn, S. Quabis, and G. Leuchs, Sharper focus for a radially polarized light beam, Phys. Rev. Lett. **91**, 233901 (2003).

[11] F. Cardano, E. Karimi, L. Marrucci, C. de Lisio, and E. Santamato, Generation and dynamics of

optical beams with polarization singularities, Opt. Express **21**, 8815 (2013).

[12] K.Y. Bliokh, F.J. Rodríguez-Fortuño, F. Nori, and V. Zayats, Spin–orbit interactions of light, Nat. Photonics **9**, 796 (2015).

[13] T.H.R. Skyrme, A non-linear field theory, Proc. R. Soc. Lond. A **260**, 127 (1961).

[14] C.D. Parmee, M.R. Dennis, and J. Ruostekoski, Optical excitations of skyrmions, knotted solitons, and defects in atoms, Commun. Phys. **5**, 1 (2022).

[15] Y. Shen, E.C. Martínez, and C. Rosales-Guzmán, Generation of tunable optical skyrmions on Skyrme-Poincaré sphere, arXiv: 2107.04394 (2021).

[16] R. Gutiérrez-Cuevas and E. Pisanty, Optical polarization skyrmionic fields in free space, J. Opt. **23**, 024004 (2021).

[17] L. Du, A. Yang, A.V. Zayats, and X. Yuan, Deep-subwavelength features of photonic skyrmions in a confined electromagnetic field with orbital angular momentum, Nat. Phys. **15**, 650 (2019).

[18] D. Marco, I. Herrera, S. Brasselet, and M.A. Alonso, Propagation-invariant optical meron lattices, ACS Photonics **11**, 2397 (2024).

[19] Y. Shen, Y. Hou, N. Papasimakis, and N.I. Zheludev, Supertoroidal light pulses as electromagnetic skyrmions propagating in free space, Nat. Commun. **12**, 5891 (2021).

[20] R. Droop, D. Ehrmanntraut, and C. Denz, Transverse energy flow in an optical Skyrmionic Hopfion, Opt. Express **31**, 11185 (2023).

[21] H. Guo, T. Das, H. Wu, V. Dev, Z. Zhu, and Y. Shen, Self-healing of optical skyrmionic beams, J. Opt. **27**, 025604 (2025).

[22] L. Chen, Y. Shen, X.Y. Li, Z. Gu, J.L. Su, Q. Xiao, Q. Huang, S.L. Qin, Q. Ma, J.W. You, et al., Programmable skyrmions for robust communication and intelligent sensing, arXiv:2507.05944 (2025).

[23] S. Orlov, K. Regelskis, V. Smilgevičius, and A. Stabinis, Propagation of Bessel beams carrying optical vortices, Opt. Commun. **209**, 155 (2002).

[24] J. Berškys and S. Orlov, Accelerating Airy beams with particle-like polarization topologies and free-space bimeronic lattices, Opt. Lett. **48**, 1168 (2023).

[25] D. Marco, I. Herrera, S. Brasselet, and M.A. Alonso, Periodic skyrmionic textures via conformal cartographic projections, APL Photonics **9** (2024).

[26] X. Lei, A. Yang, P. Shi, Z. Xie, L. Du, A.V. Zayats, and X.Yuan, Photonic spin lattices: Symmetry constraints for skyrmion and meron topologies, Phys. Rev. Lett. **127**, 237403 (2021).

[27] H. Wu, W. Zhou, Z. Zhu, and Y. Shen, Optical skyrmion lattices accelerating in a free-space mode, APL Photonics **10** (2025).

[28] A. Hansen, J.T. Schultz, and N.P. Bigelow, Singular atom optics with spinor Bose–Einstein condensates, Optica **3**, 355 (2016).

[29] L. Han, C. Addiego, S. Prokhorenko, M. Wang, H. Fu, Y. Nahas, X. Yan, S. Cai, T. Wei, Y. Fang, et al., High-density switchable skyrmion-like polar nanodomains integrated on silicon, Nature **603**, 63 (2022).

[30] Z. Wan, H. Wang, Q. Liu, X. Fu, and Y. Shen, Ultra-degree-of-freedom structured light for ultracapacity information carriers, ACS Photonics **10**, 2149 (2023).

[31] R. Tamura, P. Kumar, A.S. Rao, K. Tsuda, F. Getzlaff, K. Miyamoto, N.M. Litchinitser, and T. Omatsu, Direct imprint of optical skyrmions in azopolymers as photoinduced relief structures, APL Photonics **9** (2024).

[32] J.A. Stratton, *Electromagnetic Theory*, IEEE Press Series on Electromagnetic Wave Theory, Vol. 33 (John Wiley & Sons, 2007).

[33] P.M. Morse and H. Feshbach, *Methods of Theoretical Physics* (Technology Press, 1946).

[34] T.H.R. Skyrme, A unified field theory of mesons and baryons, Nucl. Phys. **31**, 556 (1962).

NEVIENALYTIŠKAI POLIARIZUOTI AIRY PLUOŠTAI IR JŲ GREITĖJANČIOS OPTINIŲ KVAZIDALELIŲ GARDELĖS

J. Berškys, K. Laurinavičius, S. Orlov

Valstybinio mokslinių tyrimų instituto Fizinių ir technologijos mokslų centro Koherentinės optikos laboratorija, Vilnius, Lietuva

Santrauka

Darbe tiriama sferiškai poliarizuotų Airy tipo pluoštų topologinėms dalelėms būdinga lauko struktūra. Šie pluoštai pasižymi taškinio tipo singuliarumu židinio plokštumoje ir išlaiko skaliariniams Airy pluoštams būdingą parabolinę, greitėjančią sklidimo trajektoriją. Pirmiausia apžvelgiama metodika, leidžianti iš skaliarinių laukų sprendinių gauti elektromagnetinių ortogonalių vektorinių modų bazę. Tokie vektoriniai pluoštai yra Maksvelo lygčių sprendiniai. Taikant šią metodiką, parenkamas vektorinių modų simetriją nusakantis vektorius, nukreiptas radiališkai sferinėje koordinačių bazėje. Tokio vektoriaus pasirinkimas lemia taškinio tipo singuliarumą pluošto židinyje. Taip pat pateikiami šių laukų erdviniai intensyvumo profiliai dviem ortogonaliems vektorinių laukų sprendiniams – **M** ir **N** – bei analizuojama jų poliarizacija. Matyti, kad atvaizdavus amplitudės modulį ir poliarizacijos kryptį, šie laukai įgauna skersinei elektrinei (TE) ir magnetinei (TM) modoms būdingą struktūrą ir yra radiališkai bei azimutiškai poliarizuoti. Nagrinėjant šių laukų topologiją, apskaičiuojamas atitinkamo lauko skirmioninis tankis. Analizuojant TM modos elektrinio lauko domeną, aptinkamos su pagreičiu judančios topologinių lauko struktūrų gardelės, kurių mazgai atitinka Bloch ir Néel tipo bimeronines topologines kvazidaleles. Taip pat Poyntingo vektoriaus domene aptiktos Néel ir priešingo (anti) tipo skirmioninės lauko struktūros, judančios pluošte su pagreičiu ir sudarančios gardelę.